Distributed Non-Negative Tensor Train Decomposition

Manish Bhattarai
Theoretical Division
Los Alamos National Laboratory
Los Alamos, NM, USA
ceodspspectrum@lanl.gov

Gopinath Chennupati
Information Sciences
Los Alamos National Laboratory
Los Alamos, NM, USA
gchennupati@lanl.gov

Erik Skau
Information Sciences
Los Alamos National Laboratory
Los Alamos, NM, USA
ewskau@lanl.gov

Raviteja Vangara
Theoretical Division
Los Alamos National Laboratory
Los Alamos, NM, USA
rvangara@lanl.gov

Hristo Djidjev
Information Sciences
Los Alamos National Laboratory
Los Alamos, NM, USA
djidjev@lanl.gov

Boian S. Alexandrov
Theoretical Division
Los Alamos National Laboratory
Los Alamos, NM, USA
boian@lanl.gov

arXiv:2008.01340v1 [cs.DC] 4 Aug 2020

***Abstract*—The era of exascale computing opens new venues for innovations and discoveries in many scientific, engineering, and commercial fields. However, with the exaflops also come the extra-large high-dimensional data generated by high-performance computing. High-dimensional data is presented as multidimensional arrays, aka tensors. The presence of latent (not directly observable) structures in the tensor allows a unique representation and compression of the data by classical tensor factorization techniques. However, the classical tensor methods are not always stable or they can be exponential in their memory requirements, which makes them not suitable for high-dimensional tensors. Tensor train (TT) is a state-of-the-art tensor network introduced for factorization of high-dimensional tensors. TT transforms the initial high-dimensional tensor in a network of three-dimensional tensors that requires only a linear storage. Many real-world data, such as, density, temperature, population, probability, etc., are non-negative and for an easy interpretation, the algorithms preserving non-negativity are preferred. Here, we introduce a distributed non-negative tensor-train and demonstrate its scalability and the compression on synthetic and real-world big datasets.**

***Index Terms*—tensor networks, non-negative factorization, tensor train, compression**

I. Introduction

Extra-large volumes of data are constantly being generated nowadays in areas such as personalized medicine, biology, space, nuclear science, climate and in many other fields. A common way to store and use such data is to first reduce its size without losing important information. Unfortunately, the classical compression techniques that are searching for repeated patterns often cannot be used when the data comes from high-performance computing (HPC) simulations that require a relatively high-precision and need a high accuracy of prediction. Such simulation data is usually high-dimensional and is naturally represented by tensors, i.e., as multi-dimensional arrays. Tensors in such applications typically represent multiple concurrent *latent* (not-directly observable) processes (e.g., explosions, earth-quakes, etc.) of the simulated phenomenon, imprinting their signatures in various simulated variables (such as temperature, pressure, density, etc.) in different dimensions (e.g., space/time). Despite the differences, most of the simulated phenomena share the property that the information content of the generated data is quite low, i.e., it can be represented by a low number of parameters, which are however not known a priori and are implicit in the data. Classical tensor decomposition techniques such as Tucker Decomposition [1] and Canonical Polyadic Decompositions (CPD) [2], can extract the latent structures and parameters describing the data, which allows a new type of compression. For instance, if we consider a d-dimensional tensor with n elements in each dimension and a *tensor rank* r, CPD allows the representation with the smallest number of parameters, $\mathcal{O}(dnr)$, among all tensor decomposition methods. Unfortunately, finding the canonical rank is an NP-hard problem [3] and, moreover, the approximation with a fixed rank can be ill-posed [4]. For the same tensor, the Tucker decomposition is stable and will have $\mathcal{O}(dnr+r^d)$ number of parameters. Tucker decomposition was previously proposed for compression of large scientific data and it demonstrated an excellent compressibility [5]. However, for tensors of a higher dimension, d (say 10 or more), Tucker decomposition is not feasible since the memory and amount of operations grow exponentially with the tensor dimension d.

Tensor train (TT) has been introduced in [6] as a method for decomposition of extra large and high-dimensional tensors targeting application in the solution of partial differential equations. TT is a state-of-the-art tensor network based on Singular Value Decomposition (SVD) process that parameterizes the initial high-dimensional tensor by a network of three-dimensional tensors [7]. Figure 1 represents a TT decomposition for a four-dimensional tensor. TT (also known in other areas as a matrix product state [8]) is stable and requires only a linear storage in d with $\mathcal{O}(dnr^2)$ parameters, making it suitable for compression of high-dimensional tensors [9].

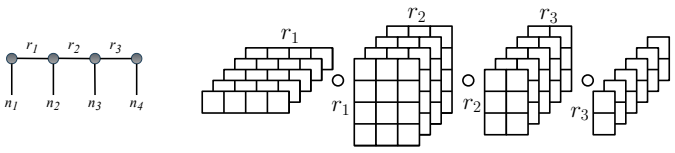


Fig. 1: (left) A graphical representation of a TT for a 4-dimensional tensor. A core is represented by a circle, while arms indicate the modes of the tensor and rank indices. The first and last TT cores are matrices, whereas the rest are 3-dimensional tensors. (right) Example of a TT for a $5\times4\times5\times6$ tensor with *tensor train rank* ($r_1 = 4, r_2 = 3, r_3 = 2$).

Many real-world types of data, such as density, temperature, population, probability, etc., are non-negative and hence algorithms that preserve the non-negativity are preferred in order to retain the interpretability and meaning of the compressed data. Nonnegative factorization is used as a model for recovering latent structures in such data and it has some additional useful features. For instance, with interpretation of the elements of the data as conditional probabilities, one can make use of the duality between latent graphical models and tensor networks [10], [11] to obtain a graphical model representation of the data, thereby allowing suitable algorithms for graphical models to be applied for tensor analysis. Graphical models have many applications in finance, machine learning, computer vision, speech recognition, and bioinformatics. Moreover, in contrast with the general case, the nonnegative best rank approximation of a tensor *always* exists [12] and it is almost always *unique* [13], which are useful properties for tensor data analysis.

Due to the large input size and the additional computational efforts needed to ensure the nonnegativity of the resulted low-dimensional factors, nonnegative tensor train (nTT) cannot be applied to data coming from many real-life applications, unless massive parallelism is used. Unfortunately, no distributed algorithm for computing an nTT decomposition has been designed yet. In this paper, we introduce such distributed nTT algorithm and analyze its performance. Our algorithm is based on distributed implementation of nonnegative matrix factorization (NMF) and tensor unfolding and reshaping operations. In the next sections, we describe details of the algorithm, its implementation, and analyze its compression ability and scalability on synthetic and real-world datasets.

II. Background

Tensor train (TT) networks were first introduced by Oseledets in [6]. Unlike other tensor decompositions, TT, being based on a sequence of SVD operations, is easy to compute and does not suffer from the curse of dimensionality. Based on EckartYoung theorem [14], SVD can be used to provide the best low-rank approximation; hence, we expect that TT (which ignores the nonnegativity) will lead to excellent compression results. From the number of parameters that Tucker decomposition and TT require, we can also conclude that the compresibility of TT will be better that the compresibility of Tucker decomposition. In fact, Figure 2 shows this phenomenon, where we present the compression versus relative error results for TT, nTT, Tucker and nonnegative Tucker decompositions, performed for the same synthetically generated tensor calculated with [15], [16]. Importantly, although with the smallest number of parameters, CP decomposition uses a single rank for all modes, which makes it less robust compared to TT and Tucker decompositions.

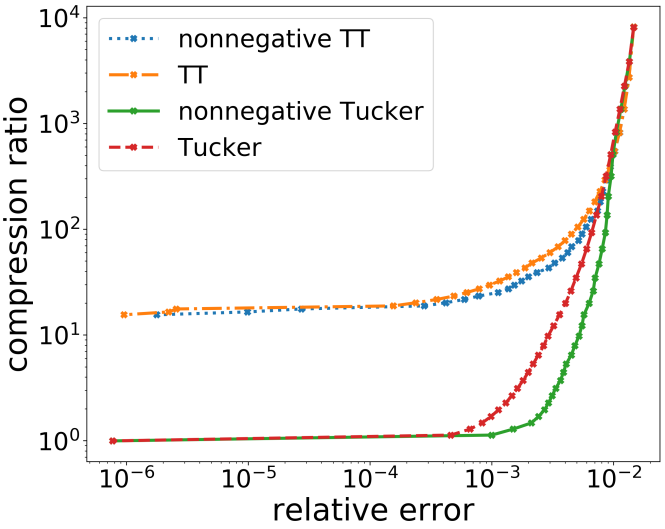


Fig. 2: Compression versus relative error for various algorithms on a synthetic data of dimensions 32 x 32 x 32 x 32.

The main factor to be taken into consideration when computing tensor train decompositions is the tradeoff between relative error and the tensor train rank [17]. Decompositions of specified ranks could have either a large computational complexity, or may result in a large error. A number of algorithms to compute tensor trains exists (each addressing this issue in a different way), such as, the sequential approach known as TT-SVD [7], Alternating Least Squares (ALS) algorithms [18], and Density Matrix Renormalization Group (DMRG) algorithms from quantum physics [19], [20].

A number of distributed TT algorithms [21], [22], [23] exist in the literature. An application of a new out-of-memory algorithm for truncated SVD computation for use in the TT algorithms, targeting tensors so large that they cannot fit in the memory, was also proposed in [24]. Recently, a MapReduce-based distributed TT algorithm for large-scale dimension reduction and classification was introduced in [21]. However, the proposed framework is unable to achieve significant scalability compared to non-distributed implementation. Next, [22] used a blocking strategy for distributed TT, where the reshape operation of the tensor block is done locally before decomposition. They compute the relative error between the TT cores calculated in a distributed manner and the non-distributed approach. In such cases, the paper fails to evaluate the correctness of the framework for large-sized tensors where the non-distributed approach cannot be applied. Recently, [23] proposed a distributed TT for processing Internet of things (IoT) data. Similar to [22], this framework has the limitations

on the ability to compute the final reconstruction error from the factors of a large scale tensor.

Nonnegative tensor train is a much less explored topic, with only a handful of published works [25], [26], [27].

In [25], Lee *et. al.* proposed a nonnegative tensor train and provide an NTT-HALS algorithm to compute it. NTT-HALS aims to minimize the Frobenius norm reconstruction error for a given tensor train rank by using a Hierarchical Alternating Least Squares (HALS) procedure. The authors demonstrated that the storage cost of their NTT-HALS decomposition is significantly lower than a corresponding nonnegative Tucker decomposition. Due to its computational complexity, the NTT-HALS algorithm is ill suited to large high-dimensional tensors. In [27] the authors propose an algorithm called NTTF, which relies on successive unfoldings and NMF approximations. That algorithm can accommodate a desired relative error by ensuring that each NMF approximation achieves a certain accuracy. This is computationally efficient approach, but it can result in unbalanced and large tensor train ranks. Finally, in [26], Shcherbakova proposes a NTT-MU algorithm similar in goal to [25], but based on a DMRG algorithm to additionally minimize the tensor train ranks. DMRG-based algorithms simultaneously optimize over consecutive pairs of tensors in the train, this allows the tensor train rank between the pair to be adjusted. However, the proposed algorithm utilizes multiplicative update to ensure nonnegativity, which suffers from the inability to converge to a high accuracy.

TABLE I: Notation

Notation	Dimensions	Description
$\boldsymbol{\mathcal{A}}$	$n_1 \times \ldots \times n_d$	Tensor of interest
$\boldsymbol{\mathcal{G}}^{(i)}$	$r_{i-1} \times n_i \times r_i$	Tensor train core
p_i	scalar	Processor count along each dimension
$\boldsymbol{\mathcal{A}}^{(i_1,\ldots,i_d)}$	$\frac{n_1}{p_1} \times \ldots \times \frac{n_d}{p_d}$	Distributed block of the tensor
m	scalar	Number of rows of a matrix
n	scalar	Number of columns of a matrix
$\boldsymbol{X}$	$m \times n$	Input matrix to NMF
p_r	scalar	Proc. count along rows of matrix
p_c	scalar	Proc. count along columns of matrix
$\boldsymbol{X}^{(i,j)}$	$\frac{m}{p_r} \times \frac{n}{p_c}$	Distributed block of matrix
r	scalar	Low rank
$\boldsymbol{W}$	$m \times r$	Left low rank factor
$\boldsymbol{H}$	$r \times n$	Right low rank factor
p	scalar	Total processor count, $p = \prod_{i=1}^{d} p_i$
$(\boldsymbol{W^i})^{\boldsymbol{j}}$	$\frac{m}{p} \times r$	Left low rank factor on $(i,j)^{th}$ processor
$(\boldsymbol{H^j})^{\boldsymbol{i}}$	$r \times \frac{n}{p}$	Right low rank factor on $(i,j)^{th}$ processor
$\boldsymbol{W}^{(i)}$	$\frac{m}{p_r} \times r$	Block of factor W corresponding to block $\boldsymbol{X}^{(i,j)}$
$\boldsymbol{H}^{(j)}$	$r \times \frac{n}{p_c}$	Block of factor H corresponding to block $\boldsymbol{X}^{(i,j)}$

III. Algorithmic Details

The tensor-train format is an efficient representation of a higher dimensional tensor in terms of storage requirements and computational robustness [6],[28]. Tensor train representation achieves such performance metrics by combining the major advantages of the Canonical format and the Tucker format [29]. Tensor train decomposes a d-dimensional tensor $\boldsymbol{\mathcal{A}} \in \mathbb{R}^{n_1 \times \ldots \times n_d}$ into d 3-dimensional tensors $\boldsymbol{\mathcal{G}}^{(i)} \in \mathbb{R}^{r_{i-1} \times n_i \times r_i}$, where $r_0 = r_d = 1$ (so $\boldsymbol{\mathcal{G}}^{(1)}$ and $\boldsymbol{\mathcal{G}}^{(d)}$ are actually matrices) and $r_k \geq 1$ for $k = 1, ..., d-1$, such that

$$\boldsymbol{\mathcal{A}} = \boldsymbol{\mathcal{G}}^{(1)} \circ \boldsymbol{\mathcal{G}}^{(2)} \circ \ldots \circ \boldsymbol{\mathcal{G}}^{(d)}, \tag{1}$$

where $\boldsymbol{\mathcal{A}} \circ \boldsymbol{\mathcal{B}}$ is used to define tensor-tensor multiplication with contraction along the last axis of $\boldsymbol{\mathcal{A}}$ and the first axis of $\boldsymbol{\mathcal{B}}$, $(\boldsymbol{\mathcal{A}} \circ \boldsymbol{\mathcal{B}})_{i_1,i_2,\ldots,i_{d-1},j_2,j_3,\ldots,j_d} = \sum_k \boldsymbol{\mathcal{A}}_{i_1,\ldots,i_{d-1},k} \boldsymbol{\mathcal{B}}_{k,j_1,j_2,\ldots,j_d}$. Here, the 3-dimensional tensors $\boldsymbol{\mathcal{G}}^{(i)}$ are called *TT cores* and the numbers $r_1, \ldots, r_{d-1}$ are called *TT ranks*. Based on the above, any element of the tensor $\boldsymbol{\mathcal{A}}$ can be further be represented as

$$\boldsymbol{\mathcal{A}}_{i_1,\ldots,i_d} = \sum_{k_1,\ldots,k_{d-1}}^{r_1,\ldots,r_{d-1}} \boldsymbol{\mathcal{G}}^{(1)}_{i_1,k_1} \boldsymbol{\mathcal{G}}^{(2)}_{k_1,i_2,k_2} \cdots \boldsymbol{\mathcal{G}}^{(d)}_{k_{d-1},i_d}. \tag{2}$$

Table I shows the notations used in the paper.

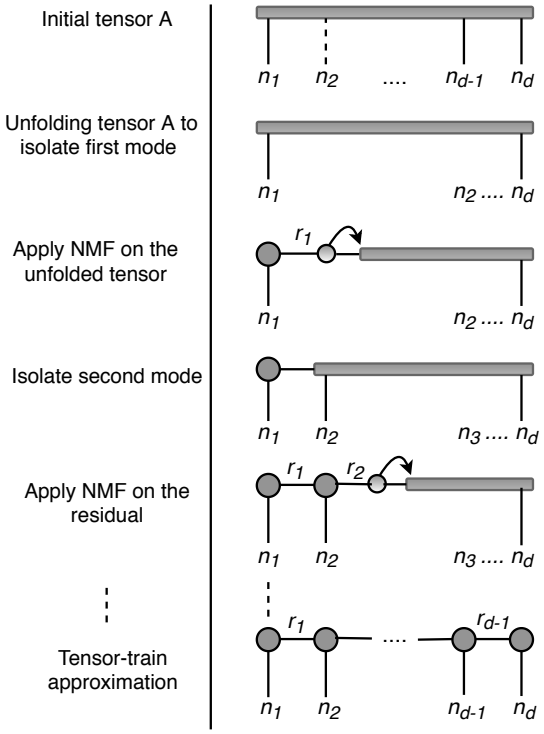


Fig. 3: The decomposition procedure of a tensor into a TT format iteratively isolates the next mode and applies NMF to get the next factor. The TT cores are represented by circles, while the remaining unfactored matrix is represented by a bar.

A. Non-Negative Tensor Train

Figure 3 illustrates the construction of a d-dimensional TT. Given a d-dimensional tensor $\boldsymbol{\mathcal{A}} \in \mathbb{R}^{n_1 \times n_2 \times \ldots \times n_d}$, the first step of TT is to isolate the first mode of $\boldsymbol{\mathcal{A}}$ with left unfolding to produce a matrix $\boldsymbol{X} \in \mathbb{R}^{n_1 \times n_2 n_3 \ldots n_d}$. NMF is used to reduce $\boldsymbol{X}$ to its corresponding factors $\boldsymbol{W} \in \mathbb{R}^{n_1 \times r_1}$ and

Algorithm 1 $\boldsymbol{X}^{(i,j)} = \text{distReshape}(\boldsymbol{\mathcal{A}}^{(i_i,\ldots,i_d)}, [m,n], [p_i,p_j])$ – Distributed reshaping of tensor $\boldsymbol{\mathcal{A}}$ into $\boldsymbol{X}$

Require: : Tensor $\boldsymbol{\mathcal{A}}^{(i_1,i_2,\ldots,i_d)} \in \mathbb{R}^{\frac{n_1}{p_1}\times\ldots\times\frac{n_d}{p_d}}$,target matrix shape $m \times n$ and target processor grid size $p_r \times p_c$.

Each MPI rank writes a block of $\boldsymbol{\mathcal{A}}^{(i_1,i_2,\ldots,i_d)}$.

Perform global reshaping of the tensor from tensor dimensions $n_1 \times n_2 \times \ldots \times n_d$ into $m \times n$ i.e $\boldsymbol{\mathcal{X}} = reshape(\boldsymbol{\mathcal{A}}, [m_1, m_2, ...m_k])$.

Compute in-memory data $\boldsymbol{X}^{(i,j)}$ for each MPI rank from the reshaped tensor $\boldsymbol{X}$ where size of $\boldsymbol{X}^{(i,j)} = \frac{m}{p_r} \times \frac{n}{p_c}$

Ensure: $\boldsymbol{X} \in \mathbb{R}^{m\times n}$ and $\boldsymbol{X}^{(i,j)} \in \mathbb{R}^{\frac{m}{p_r}\times\frac{n}{p_c}}$

Algorithm 2 $\boldsymbol{\mathcal{G}}_1, \boldsymbol{\mathcal{G}}_2, \ldots, \boldsymbol{\mathcal{G}}_d = \text{distnTT}(\boldsymbol{\mathcal{A}}^{(i_1,i_2,\ldots,i_d)}, \epsilon)$ – Distributed non negative tensor train algorithm

Require: Tensor $\boldsymbol{\mathcal{A}}^{(i_1,i_2,\ldots,i_d)} \in \mathbb{R}^{\frac{n_1}{p_1}\times\ldots\times\frac{n_d}{p_d}}$ and threshold ϵ.

Set $r_0 = r_d = 1$

Set $\boldsymbol{A}^{(i,j)} = \text{distReshape}(\boldsymbol{\mathcal{A}}^{(i_1,i_2,\ldots,i_d)}, [n_1, \frac{S}{n_1}], [p_1, p/p_1])$ ▷ $S = n_1 \times n_2 \ldots \times n_d$ and $p = p_1 \times p_2 \ldots \times p_d$

for l in 1 to $d-1$ **do**

  $\boldsymbol{X}^{(i,j)} = \text{distReshape}(\boldsymbol{A}^{(i,j)}, [r_{l-1}n_l, \frac{S}{r_{l-1}n_l}], [p_1, p/p_1])$ ▷ $S = n_l \times n_{l+1} \ldots \times n_d$

  $\boldsymbol{U}^{(i,j)}\boldsymbol{\Sigma}\boldsymbol{V}^{(\boldsymbol{i},\boldsymbol{j})\boldsymbol{T}} = \text{distSVD}(\boldsymbol{X}^{(i,j)})$ ▷ $\Sigma \in \mathbb{R}^{N\times N}$

  Choose r_l smallest k such that $\frac{\sqrt{\sigma_{k+1}^2+\ldots+\sigma_N^2}}{\sqrt{\sigma_1^2+\ldots+\sigma_N^2}} \leq \epsilon$

  $(\boldsymbol{W^i})^{\boldsymbol{j}}, (\boldsymbol{H^j})^{\boldsymbol{i}} = \text{distBCDnmf}(\boldsymbol{X}^{(i,j)}, r_l)$

  $\boldsymbol{\mathcal{G}}^{(l)} = \text{reshape}(\text{all_gather}((\boldsymbol{W^i})^{\boldsymbol{j}}), [r_{l-1}, n_l, r_l])$ ▷ Perform global all_gather on $(\boldsymbol{W^i})^{\boldsymbol{j}}$ along row-wise distribution. $\mathbb{R}^{r_{l-1}\times n_l \times r_l}$

  $\boldsymbol{A}^{(i,j)} = (\boldsymbol{H^j})^{\boldsymbol{i}}$ ▷ $\in \mathbb{R}^{r_l \times n_{l+1}\ldots n_d}$ is 1D-distributed

end for

Set d-th core to $\boldsymbol{\mathcal{G}}^{(d)}_{:,:,1} = \text{all_gather}(\boldsymbol{A}^{(i,j)})$ ▷ Perform global all_gather on $\boldsymbol{A}^{(i,j)}$ along column-wise distribution

Ensure: Approximation $\boldsymbol{\mathcal{G}}^{(1)} \circ \boldsymbol{\mathcal{G}}^{(2)} \circ \ldots \circ \boldsymbol{\mathcal{G}}^{(d)}$ of $\boldsymbol{\mathcal{A}}$ in TT format with cores $\boldsymbol{\mathcal{G}}^{(1)}, \boldsymbol{\mathcal{G}}^{(2)}, \ldots, \boldsymbol{\mathcal{G}}^{(d)}$ and TT ranks $r_0, r_1, ..., r_d$

$\boldsymbol{H} \in \mathbb{R}^{r_1 \times n_2 n_3 \ldots n_d}$. The rank of this NMF decomposition, r_1, is selected by an SVD-based heuristic, namely, r_1 is selected by choosing it to be equal to the smallest k such that $\sqrt{\sigma_{k+1}^2 + \ldots + \sigma_N^2}/\sqrt{\sigma_1^2 + \ldots + \sigma_N^2} \leq \epsilon$, where σ_i is the i^{th} singular value of $\boldsymbol{X}$ and $N = \min(n_1, n_2 n_3 \ldots n_d)$. The singular values decrease and reach a plateau, separating a cluster of non-latent dimensions ($r \geq r_{s+1}$) to that of latent ones ($r \leq r_s$). The number of these larger singular values is used to calculate the effective rank of a matrix [30] as well in Bayesian PCA [31]. There are other sophisticated approaches to identify latent dimensionality of NMF [32], which could be included in our method. The left NMF factor W is the first core of the non-negative tensor train decomposition of $\mathbf{X}$. The right NMF factor $\boldsymbol{H}$ is further reshaped to $\boldsymbol{X} \in \mathbb{R}^{r_1 n_2 \times n_3 \times n_4 \times \ldots \times n_d}$. The procedure is repeated until the final NMF factor $\boldsymbol{H} \in \mathbb{R}^{r_{d-1}\times n_d}$, i.e., core $\boldsymbol{\mathcal{G}}^{(d)}$ of nTT is obtained.

Algorithm 3 $(\boldsymbol{W^i})^{\boldsymbol{j}}, (\boldsymbol{H^j})^{\boldsymbol{i}} = \text{distBCDnmf}(\boldsymbol{X}^{(i,j)}, r)$ – Distributed BCD NMF algorithm

Require: $\boldsymbol{X}^{(i,j)} \in \mathbb{R}_+^{\frac{m}{p_r}\times\frac{n}{p_c}}$ and desired rank r.

Initialize $(\boldsymbol{W^i})^{\boldsymbol{j}}$, $(\boldsymbol{H^j})^{\boldsymbol{i}} = \text{rand}(\frac{m}{p}, r)$, $\text{rand}(r, \frac{n}{p})$

$(\boldsymbol{W^i})^{\boldsymbol{j}}_m$, $(\boldsymbol{H^j})^{\boldsymbol{i}}_m = \frac{(\boldsymbol{W^i})^{\boldsymbol{j}}}{||\boldsymbol{W}||}\sqrt{||\boldsymbol{X}||}$, $\frac{(\boldsymbol{H^j})^{\boldsymbol{i}}}{||\boldsymbol{H}||}\sqrt{||\boldsymbol{X}||}$ ▷ Normalize

$\boldsymbol{HH^T}, ((\boldsymbol{XH^T})^i)^j = \text{distMM}^{\text{T}}((\boldsymbol{H^j})^{\boldsymbol{i}}_{\boldsymbol{m}}), \text{distXH}^{\text{T}}(\boldsymbol{X}^{(i,j)}, (\boldsymbol{H^j})^{\boldsymbol{i}}_{\boldsymbol{m}})$

t, obj = 1.0, $\frac{1}{2}||X||$ ▷ Correction of $\boldsymbol{W}$ and $\boldsymbol{H}$

for l in max_iters **do**

/* Update W given H */

  $(\boldsymbol{W_m HH^T})^{\boldsymbol{i}})^{\boldsymbol{j}} = (\boldsymbol{W^i})^{\boldsymbol{j}}_m \boldsymbol{HH^T}$ ▷ i^{th} proc $\mathbb{R}_+^{\frac{m}{p}\times r}$

  $(\boldsymbol{G^i_W})^{\boldsymbol{j}} = (\boldsymbol{W_m HH^T})^{\boldsymbol{i}})^{\boldsymbol{j}} - ((\boldsymbol{XH^T})^i)^j$ ▷ $(\boldsymbol{G^i_W})^{\boldsymbol{j}} \in \mathbb{R}_+^{\frac{m}{p}\times r}$

  $(\boldsymbol{W^i})^{\boldsymbol{j}} = \max(0, \frac{(\boldsymbol{W^i})^{\boldsymbol{j}}_{\boldsymbol{m}}}{||\boldsymbol{HH^T}||})$

  $(\boldsymbol{W^i})^{\boldsymbol{j}} /= ||\boldsymbol{W}||_1$ ▷ Normalize with L_1 norm

  $\boldsymbol{W^T W} = \text{distMM}^{\text{T}}(((\boldsymbol{W^i})^{\boldsymbol{j}})^T)$

/* Update H given W*/

  $(\boldsymbol{W^T W H^j_m})^{\boldsymbol{i}} = \boldsymbol{W^T W} (\boldsymbol{H^j})^{\boldsymbol{i}}_m$ ▷ $(\boldsymbol{W^T W H^j_m})^{\boldsymbol{i}} \in \mathbb{R}_+^{r\times\frac{n}{p}}$

  $((\boldsymbol{W^T X})^j)^i = \text{distWTX}(\boldsymbol{X}^{(i,j)}, (\boldsymbol{W^i})^{\boldsymbol{j}})$

  $(\boldsymbol{G^j_H})^{\boldsymbol{i}} = (\boldsymbol{W^T W H^j_m})^{\boldsymbol{i}} - ((\boldsymbol{W^T X})^j)^i$ ▷ $(\boldsymbol{G^j_H})^{\boldsymbol{i}} \in \mathbb{R}_+^{r\times\frac{n}{p}}$

  $(\boldsymbol{H^j})^{\boldsymbol{i}} = \max(0, (\boldsymbol{H^j})^{\boldsymbol{i}}_{\boldsymbol{m}} - \frac{(\boldsymbol{G^j_H})^{\boldsymbol{i}}}{\sqrt{WTW}})$

  $\boldsymbol{HH^T} = \text{distMM}^{\text{T}}((\boldsymbol{H^j})^{\boldsymbol{i}})$

  $((\boldsymbol{XH^T})^i)^j = \text{distXH}^{\text{T}}(\boldsymbol{X}^{(i,j)}, (\boldsymbol{H^j})^{\boldsymbol{i}})$

  if $\frac{1}{2}||\boldsymbol{X} - \boldsymbol{WH}||^2 >= obj$ **then** ▷ **/* Correction */**

    $Initialize$ $(\boldsymbol{W^i})^{\boldsymbol{j}}$ and $(\boldsymbol{H^j})^{\boldsymbol{i}}$

    $\boldsymbol{HH^T} = \text{distMM}^{\text{T}}((\boldsymbol{H^j})^{\boldsymbol{i}})$

    $((\boldsymbol{XH^T})^i)^j = \text{distXH}^{\text{T}}(\boldsymbol{X}^{(i,j)}, (\boldsymbol{H^j})^{\boldsymbol{i}})$

  else ▷ **/* Extrapolation */**

    $w = (t-1)/\frac{1+\sqrt{1+4t^2}}{2}$

    $w_W = \min(w, \delta\sqrt{||\boldsymbol{HH^T_{(l-1)}}||/||\boldsymbol{HH^T}||})$

    $w_H = \min w, \delta\sqrt{||\boldsymbol{W^T W_{(l-1)}}||/||\boldsymbol{W^T W}||}$

    $(\boldsymbol{W^i})^{\boldsymbol{j}}_m = (\boldsymbol{W^i})^{\boldsymbol{j}} + w_W{}^*((\boldsymbol{W^i})^{\boldsymbol{j}} - (\boldsymbol{W^i})^{\boldsymbol{j}}_{\boldsymbol{l-1}})$

    $(\boldsymbol{H^j})^{\boldsymbol{i}}_m = (\boldsymbol{H^j})^{\boldsymbol{i}} + w_H{}^*((\boldsymbol{H^j})^{\boldsymbol{i}} - (\boldsymbol{H^j})^{\boldsymbol{i}}_{\boldsymbol{l-1}})$

    t, $obj = \frac{1+\sqrt{1+4t^2}}{2}$, $\frac{1}{2}||\boldsymbol{X} - \boldsymbol{WH}||^2$

  end if

end for

return $(\boldsymbol{W^i})^{\boldsymbol{j}}$, $(\boldsymbol{H^j})^{\boldsymbol{i}}$

Ensure: $(\boldsymbol{W^i})^{\boldsymbol{j}} \in \mathbb{R}_+^{\frac{m}{p}\times r}$ and $(\boldsymbol{H^j})^{\boldsymbol{i}} \in \mathbb{R}_+^{r\times\frac{n}{p}}$ and $\boldsymbol{W}, \boldsymbol{H} \approx \text{argmin}_{\widetilde{\boldsymbol{W}}\geq 0, \widetilde{\boldsymbol{H}}\geq 0} ||\boldsymbol{X} - \widetilde{\boldsymbol{W}}\widetilde{\boldsymbol{H}}||_F^2$

B. Distribution Strategy

Figure 4 shows the distributed TT for a 4-dimensional tensor $\boldsymbol{\mathcal{A}}$ into four cores $\boldsymbol{\mathcal{G}}^{(1)}$, $\boldsymbol{\mathcal{G}}^{(2)}$, $\boldsymbol{\mathcal{G}}^{(3)}$ and $\boldsymbol{\mathcal{G}}^{(4)}$. We choose a 4-dimensional processor grid of size $2 \times 2 \times 2 \times 2$ that divides each mode of the tensor. Considering the size of tensor $\boldsymbol{\mathcal{A}}$ is $n_1 \times n_2 \times n_3 \times n_4$, each distributed block of tensor $\boldsymbol{\mathcal{A}}^{(i_1,i_2,i_3,i_4)}$ will have a size of $\frac{n_1}{2} \times \frac{n_2}{2} \times \frac{n_3}{2} \times \frac{n_4}{2}$. We first perform a distributed reshaping/unfolding of the tensor $\boldsymbol{\mathcal{A}}$ into a matrix $\boldsymbol{X}$ of size $n_1 \times n_2 n_3 n_4$ using Zarr and Dask packages. We use a Zarr shared file system to store the tensor and the intermediate factors. Dask operates on the Zarr file object for reshaping. Dask first performs global tensor reshape operation via a lazy evaluation/call-by-need approach and then each MPI rank computes the in-memory chunk of data afterward. The

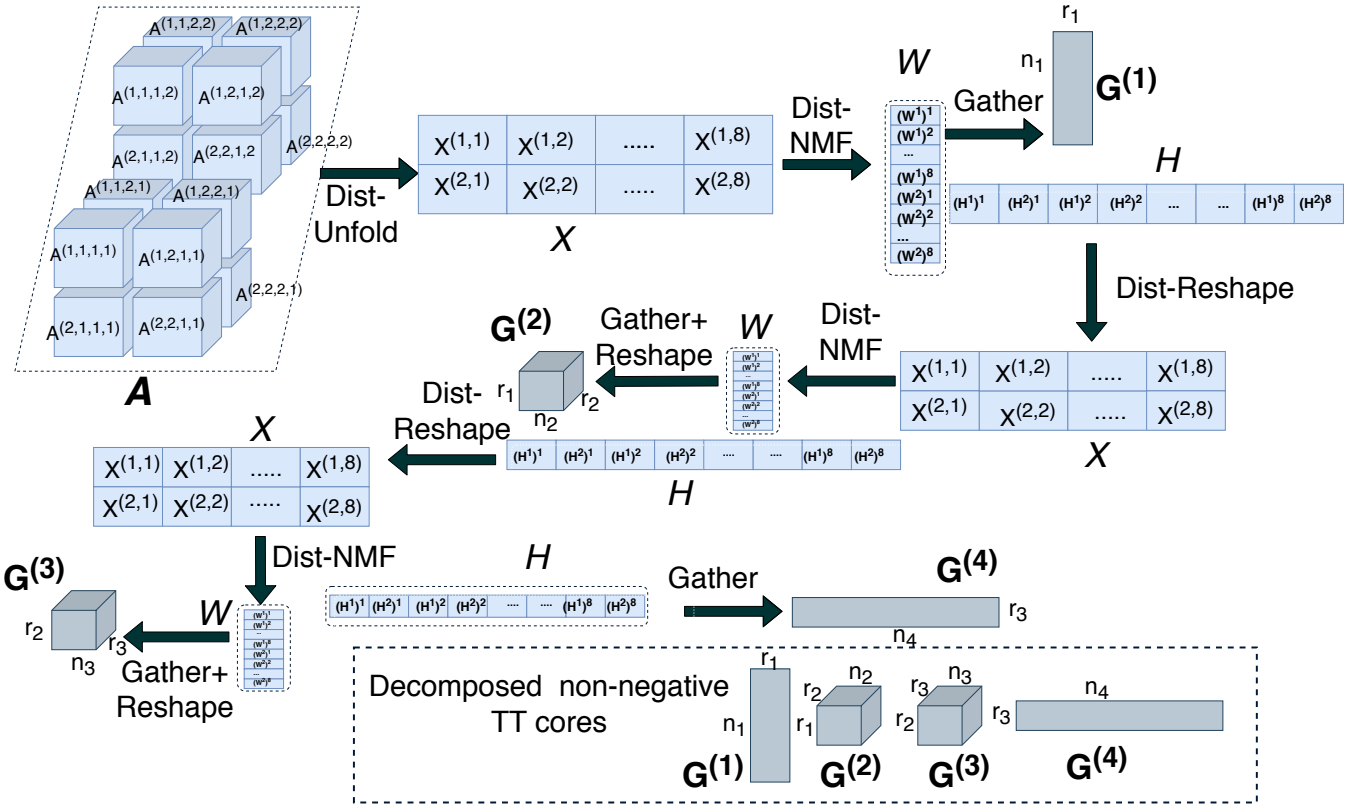


Fig. 4: Overview of distributed tensor-train decomposition of a 4D tensor with a processor grid of size 2x2x2x2.

algorithm for distributed reshape is presented in Algorithm 1. Each block of reshaped matrix $\boldsymbol{X}$ is of size $\frac{n_1}{2} \times \frac{n_2}{2}\frac{n_3}{2}\frac{n_4}{2}$. Next, we carry out the distributed SVD to find the TT rank. Then, we perform the distributed NMF algorithm with block co-ordinate descent (BCD) optimization [33] presented in Algorithm 3 on the distributed matrix $\boldsymbol{X}$. The distribution strategy of the matrix and factors for the distributed NMF is following [32]. The dist-NMF produces distributed factors matrices $\boldsymbol{W}$ and $\boldsymbol{H}$. The matrix $\boldsymbol{W}$ is gathered across the processor cores to obtain the first core tensor $\mathcal{G}^{(1)}$. Next, the 1-d distributed factor matrix $\boldsymbol{H}$ undergoes a distributed reshape as per Algorithm 1 to obtain a 2D-distributed matrix $\boldsymbol{X}$. The decomposition is carried out as described above, followed by obtaining factors $\boldsymbol{W}$ and $\boldsymbol{H}$, which are reshaped accordingly, to obtain cores $\mathcal{G}^{(i)}$ and matrices $\boldsymbol{X}$, respectively, until the final decomposition is constructed.

Algorithm 2 describes the distributed nonnegative tensor train. Along with the distributed reshape and the SVD, the next key component is the distributed BCD algorithm (see Algorithm 3). The inputs to distBCDnmf algorithm are a 2D distributed input matrix ($\boldsymbol{X}^{(i,j)}$) and the rank value (r). The algorithm returns intermediate factors, $(\boldsymbol{W^i})^j$ and $(\boldsymbol{H^j})^i$, where the second matrix is used in the reshape operation of the TT algorithm for further decomposition until the last mode of the tensor is processed. In order to get optimal intermediate factors, we employed alternating nonnegative least squares (ANLS) strategy in BCD. This alternates updating each factor while fixing the other factor to be constant.

Algorithm 4 $\boldsymbol{MM^T} = \text{distMM}^{\text{T}}((\boldsymbol{M^i})^j)$ – Distributed Gram calculation of $(\boldsymbol{M^i})^j$

Require: $(\boldsymbol{M^i})^j$ or $((\boldsymbol{M^i})^j)^T$

/* To calculate $\boldsymbol{HH^T}$ or $\boldsymbol{W^TW}$ */

1: $\boldsymbol{U}^{(i,j)} = (\boldsymbol{M^i})^j((\boldsymbol{M^i})^j)^T$ ▷ $\boldsymbol{U}^{(i,j)} \in \mathbb{R}_+^{r\times r}$

2: $\boldsymbol{MM^T} = \sum \boldsymbol{U}^{(i,j)}$ ▷ *all_reduce* across all proc

Ensure: $\boldsymbol{MM^T} \in \mathbb{R}_+^{r\times r}$

Algorithm 5 $((\boldsymbol{XH^T})^i)^j = \text{distXH}^{\text{T}}(\boldsymbol{X}^{(i,j)}, (\boldsymbol{H^j})^i)$ – Distributed matrix multiplication of $\boldsymbol{X}^{(i,j)}$ and $(\boldsymbol{H^j})^i$

Require: $\boldsymbol{X}^{(i,j)} \in \mathbb{R}_+^{\frac{m}{p_r}\times\frac{n}{p_c}}$ and $(\boldsymbol{H^j})^i \in \mathbb{R}_+^{r\times\frac{n}{p}}$

1: $\boldsymbol{H}^{(j)} = \text{all_gather}((\boldsymbol{H^j})^i)$ ▷ across processor columns, $\boldsymbol{H}^{(j)} \in \mathbb{R}_+^{r\times\frac{n}{p_c}}$

2: $\boldsymbol{V}^{(i,j)} = \boldsymbol{X}^{(i,j)}\boldsymbol{H}^{(j)\boldsymbol{T}}$ ▷ $\boldsymbol{V}^{(i,j)} \in \mathbb{R}_+^{\frac{m}{p_r}\times r}$

3: compute $(\boldsymbol{XH^T})^i = \sum \boldsymbol{V}^{(i,j)}$ ▷ *reduce-scatter* on processor rows for row-wise distribution

4: $(i,j)^{th}$ processor holds $((\boldsymbol{XH^T})^i)^j$ after *reduce-scatter*

Ensure: $((\boldsymbol{XH^T})^i)^j \in \mathbb{R}_+^{\frac{m}{p}\times r}$

The main computational steps in the distributed BCD are the calculation of matrices $\boldsymbol{W^TW}$ or $\boldsymbol{HH^T}$ (Gram matrices), $\boldsymbol{XH^T}$, and $\boldsymbol{W^TX}$. Each of these computations are being

Algorithm 6 $((\boldsymbol{W^T X})^j)^i$ = distWTX$(\boldsymbol{X}^{(i,j)}, (\boldsymbol{W^i})^j)$ – Distributed matrix multiplication of $\boldsymbol{X}^{(i,j)}$ and $(\boldsymbol{W^i})^j$

Require: $\boldsymbol{X}^{(i,j)} \in \mathbb{R}_+^{\frac{m}{p_r} \times \frac{n}{p_c}}$ and $(\boldsymbol{W^i})^j \in \mathbb{R}_+^{\frac{n}{p} \times r}$

1: $\boldsymbol{W}^{(i)}$ = all_gather$((\boldsymbol{W^i})^j)$ ▷ across processor rows, $\boldsymbol{W}^{(i)} \in \mathbb{R}_+^{\frac{n}{p_r} \times r}$

2: compute $\boldsymbol{Y}^{(i,j)} = \boldsymbol{W^{(i)T} X}^{(i,j)}$ ▷ $\boldsymbol{Y}^{(i,j)} \in \mathbb{R}_+^{r \times \frac{n}{p_c}}$

3: compute $(\boldsymbol{W^T X})^j = \sum \boldsymbol{Y}^{(i,j)}$ ▷ *reduce-scatter* on processor columns for column-wise distribution

4: $(i,j)^{th}$ processor holds $((\boldsymbol{W^T X})^j)^i$ after *reduce-scatter*

Ensure: $(\boldsymbol{W^T X})^j)^i \in \mathbb{R}_+^{r \times \frac{n}{p}}$

performed multiple times in the BCD algorithm. Therefore, we present the distributed Gram calculation in Algorithm 4, Algorithm 5 computes distributed $\boldsymbol{XH^T}$, and Algorithm 6 computes distributed $\boldsymbol{W^T X}$. We note the final conditions of BCD try to guarantee convergence to an optimal solution. In this step, the $(\boldsymbol{W^i})^j$ and $(\boldsymbol{H^j})^i$ matrices are initialized to the initial values (lines 17–20 in Algorithm 3) when the objective value of optimization is worse than the previous iteration. Otherwise, the intermediate factors are updated (lines 21–27 in Algorithm 3) accordingly with the use of a user defined hyper parameter (δ). We now evaluate our approach.

IV. Experiments and Results

We run the experiments on the HPC cluster *Grizzly*, located at Los Alamos National Laboratory (LANL). *Grizzly* has Intel Xeon Broadwell (E5-2695v4) processors with a total of 1490 compute nodes, where each node has 18-core dual socket Ivy Bridge processor. Each of the 36 processors has a clock speed of 2.1 GHz with a private L_1 and L_2 caches of sizes 64KB and 256KB. Both the sockets share an L_3 cache of size 45MB, where each node contains 128GB of memory. Grizzly uses Tri-Lab Operating System Stack (TOSS) version 3, while the interconnect is Intel *OmniPath* that uses a fat-tree topology.

Our source code is in Python, where the dependencies include Dask [1], Numpy [2], MPI4PY [3], and Zarr [4]. Our framework supports dense tensors, and we leave the sparse implementations for future releases. We use Python (v3.7.0) compiler and the OpenMPI (v2.1.2) library available on Grizzly.

A. Data Generation

We generate a synthetic tensor, say $\boldsymbol{\mathcal{A}} \in \mathbb{R}^{n_1,\ldots n_d}$, with known tensor-train ranks $r_1, \ldots, r_{d-1}$, and selected dimensions $n_1, \ldots n_d$. Each of the tensor train factors, e.g., $\boldsymbol{\mathcal{G}}_i$, gets elements sampled from a uniform distribution between 0 and 1. The tensor $\boldsymbol{\mathcal{A}}$ is then generated as a product of the TT factors and is distributed among the processors if its size is too large. Specifically, if the tensor is too large, we first generate the TT cores as described above, reshape them into matrices, and distribute them along the 1D processor grid. We then perform a distributed matrix multiplication of the factors and repeat the process until we obtain the final unfolded tensor. Then, we apply distributed reshape operation on the unfolded tensor to obtain the desired d-dimensional tensor.

B. Scalability

We evaluate the scalability of the distributed tensor train algorithm looking at both strong and weak scaling. We also analyze the scaling performance with respect to tensor train ranks. We used 16, 32, 64, 128, and 256 processors/cores for these experiments. For the scaling experiments, we collect the total time taken for the nonnegative matrix factorization for all $d-1$ factors, having fixed the number of NMF iterations to 100. This is done ten times and the average times are reported. We also report the time spent on compute, communication, and I/O operations in the TT algorithm. The computation costs are: *GR*—the local computations of a Gram matrix ($\boldsymbol{W^T W}$ or $\boldsymbol{HH^T}$), which is of size $r \times r$; *MM*matrix-matrix multiplications using local (MPI rank specific) input matrix and factor matrices; *MAD*—element-wise matrix multiplication and division operations; *Norm*—l2 norm computation of local matrices; *INIT*—initialization of factor matrices. The communication cost includes: all_gather (*AG*)—time taken for global matrix-matrix multiplications while distributing the results across all processors; all_reduce (*AR*)—the time required to compute global Gram matrices, and reduce-scatter (*RSC*)—the time to compute global matrix-matrix product using a reduce-scatter operation. We also report the breakdown of the scaling performance for distributed reshaping and I/O operations along with NMF operations.

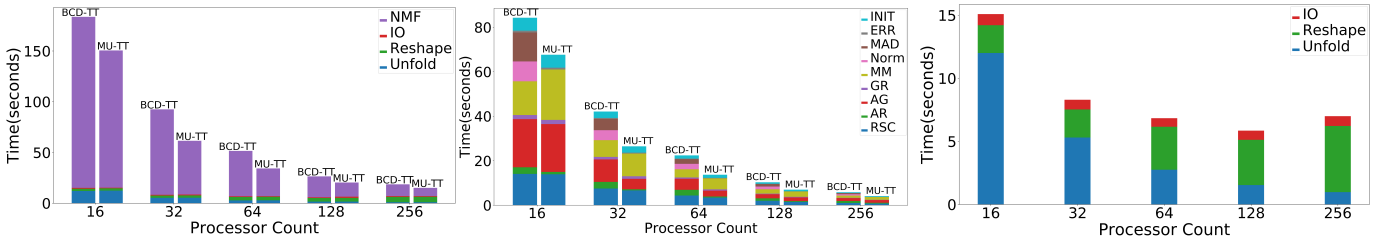
1) Strong Scaling: We use data with fixed size to be $256 \times 256 \times 256 \times 256$ (i.e. 16GB) and vary the number of processors that we use to compute the distributed tensor train decomposition. The times taken for NMF of all factors, for data operations, and the overall TT time for two NMF algorithms, the BCD (block coordinate descent) and the MU (multiplicative update) times, across processor grid of sizes $2^k \times 2 \times 2 \times 2$, where $1 \leq k \leq 5$, are presented in Figure 5.

The strong scaling experiments are run with tensor-train ranks (TT-ranks) set to be 1,10,10,10, and 1 in the respective dimensions. The scaling results show that the overall TT performance achieves better FLOPS with larger grid size as the overall running time decreases with larger processor size. The scaling saturates at larger core sizes due to the inter-processor communication and the smaller matrix operations within the local computation kernels.

2) Weak Scaling: To test the weak scaling performances of the proposed TT implementation, we report the performance per core for 100 iterations of each TT decomposition stage. Figure 6 illustrates the weak scaling performance for the proposed framework.

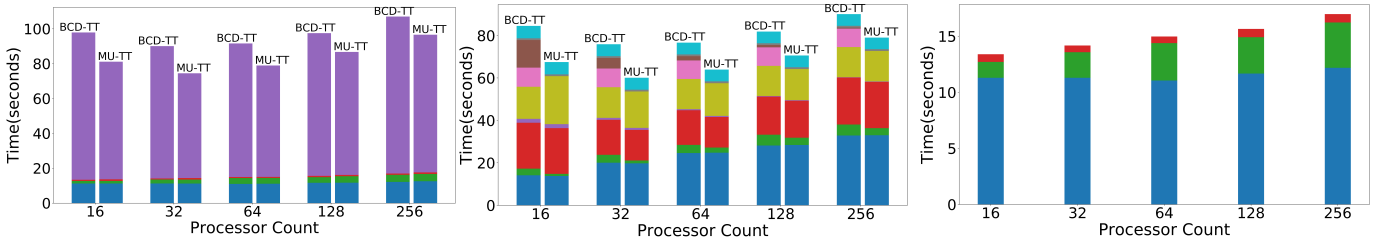
For this experiment, the size of data is fixed per processor, while we scale up the processor and the data sizes by the same factors. Similar to the strong scaling, we use processor grid of sizes $2^k \times 2 \times 2 \times 2$, where $1 \leq k \leq 5$. In addition to

[1] https://docs.dask.org/en/latest/
[2] https://numpy.org/doc/1.18/reference/index.html
[3] https://mpi4py.readthedocs.io/en/stable/
[4] https://zarr.readthedocs.io/en/stable/



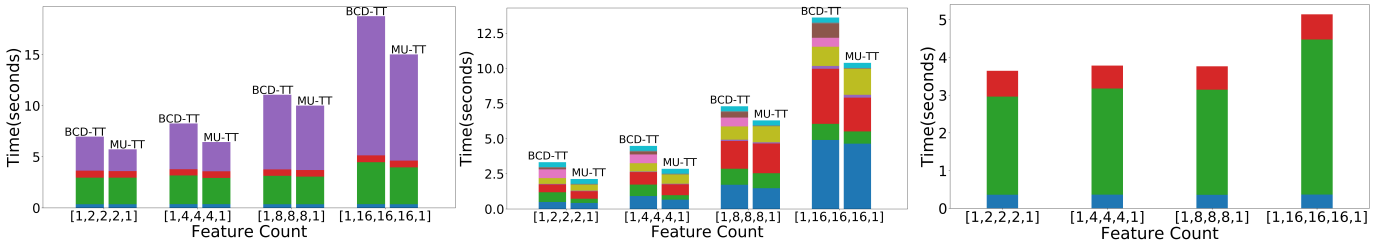
(a) Strong scaling (Overall) (b) Strong scaling (NMF) (c) Strong scaling (Data Operations)

Fig. 5: Strong scaling experiments



(a) Weak scaling (Overall) (b) Weak scaling (NMF) (c) Weak scaling (Data Operations)

Fig. 6: Weak scaling experiments



(a) Scaling with TT-ranks (Overall) (b) Scaling with TT-ranks (NMF) (c) Scaling with TT-ranks (Data Operations)

Fig. 7: Scaling experiments with respect to TT-ranks

that, we vary the data size as $256^k \times 256 \times 256 \times 256$, where $1 \leq k \leq 5$. The condition for $k = 1$ matches with the $k = 1$ setup in strong scaling. The size of data varies from 16GB to 256GB for a processor count ranging from 16 to 256. Again, the scaling performance degrades slightly for larger processors and data sizes due to the inter-nodal communications and the I/O involved.

3) Scaling with TT ranks: To demonstrate the scalability of our framework for different tensor train ranks, we fix the total number of processors to be 256 for a tensor of size $256 \times 256 \times 256 \times 256 \times 256$, and vary the inner tensor train ranks to analyze the effect of r on scaling. Figure 7 shows the scaling with TT ranks results, where each TT rank r is varied in $\{2, 4, 8, 16\}$.

C. Application to real-world dataset

1) Data Description:

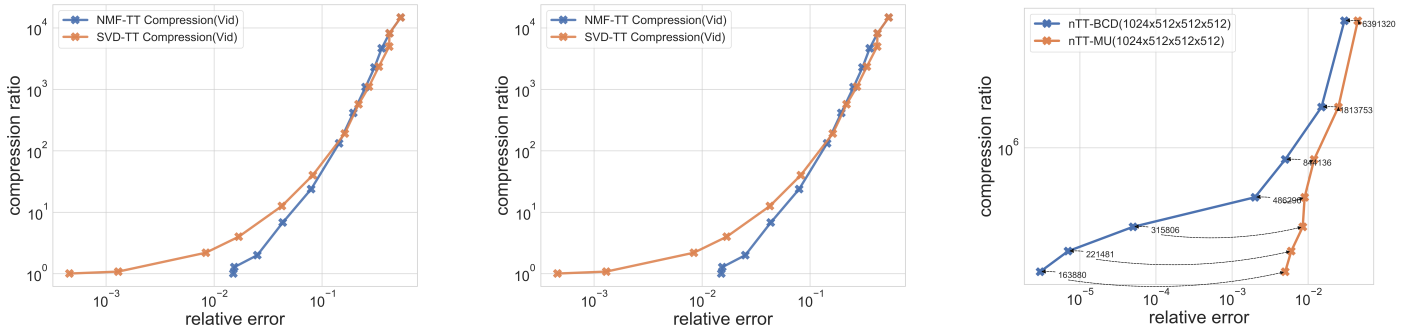
a) Extended Yale Face Dataset B: We first demonstrate the compressibility on Extended Yale Face Dataset B [34], [9], [35] that includes 38 people with 9 poses under 64 illumination conditions. Each image from the Yale Face dataset has size of 192×168, where each image is down-sampled to 48×42 for comparison with an existing method [34]. The formatted 4D tensor dimensions are $48 \times 42 \times 64 \times 38$. We also demonstrate denoising on the same dataset by adding Gaussian noise $N(0, 900)$ to each voxel of the tensor.

b) Video: The video tensor $(100 \times 260 \times 3 \times 85)$ obtained from a high-speed camera video for gun shooting [36], comprises 4 dimensions, where the first two dimensions correspond to a monochromatic image, the third dimension is the channel, and the fourth one is the frame count.

2) Compression Ratio and Reconstruction Error: For a d-way data tensor $\boldsymbol{\mathcal{A}}$ of size $n_1, n_2, ..., n_d$, the reconstructed tensor from the tensor train factors $\boldsymbol{\mathcal{G}}^{(i)}$ is given by $\tilde{\boldsymbol{\mathcal{A}}}$. Then the relative error ϵ for reconstruction is given as

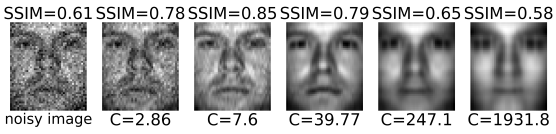
$$\epsilon = \frac{\|\boldsymbol{\mathcal{A}} - \tilde{\boldsymbol{\mathcal{A}}}\|_F}{\|\boldsymbol{\mathcal{A}}\|_F}. \tag{3}$$

If the tensor train ranks of the decomposition are $r_0 = r_d = 1$, $r_i \geq 1$ for $1 \leq i < d$, then the compression ratio is

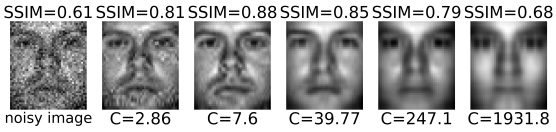


(a) (b) (c)

Fig. 8: Compression ratio vs relative error with tensor train decomposition on datasets a)Yale face b) Video c) Synthetic data (500GB)



(a)



(b)

Fig. 9: Demonstration of image denoising. (a) Denoising with SVD-TT (b) Denoising with NMF-TT

measured as

$$C = \prod_{i=1}^{d} n_i / (\sum_{i=1}^{d} n_i * r_{i-1} * r_i) \tag{4}$$

Each data point in the Figures 8a and 8b is the compression ratio C at the desired relative error ϵ at each TT decomposition stage. The targeted relative errors at each TT stage for selection of r_i was set to 0.5, 0.25, 0.125, 0.075, 0.01, 0.005 and 0.001. Lower TT rank produces higher compression and higher reconstruction error, whereas higher TT rank produces lower compression and better reconstruction. For the Yale face dataset, the compression ratio C varies from 1.13 with $\epsilon = 0.04$ to C of 2.55e4 for $\epsilon = 0.55$ with nTT. Similarly with TT, the compression ratio C varies from 1.32 with $\epsilon = 0.013$ to C of 2.55e4 for $\epsilon = 0.55$. Also, for the video dataset, the compression ratio C varies from 1.01 with $\epsilon = 0.015$ to C of 1.47e4 for $\epsilon = 0.54$ with nTT. Similarly with TT, the compression ratio C varies from 1.007 with $\epsilon = 0.0004$ to C of 1.47e4 for $\epsilon = 0.53$.

3) Application to image denoising: To demonstrate the efficacy of non-negative tensor train over the regular tensor train, we apply both techniques for the decomposition of a noisy Yale Face sample and report the denoising performance. The metric that we choose to evaluate the correctness of reconstruction compared to the noise-free sample is the structural similarity (SSIM) index [37]. SSIM is a widely used metric for image similarity measures in computer vision applications. SSIM ranges on a scale of [0,1], where 1 is the best match. In Figure 9, we report the SSIM values of the reconstructed images with respect to the noiseless ground truth image. Figure 9a corresponds to the regular tensor train based reconstruction, whereas Figure 9b corresponds to the non-negative TT based reconstruction. For both of these figures, the images from left to right correspond to the reconstructed images with decreasing TT-ranks and increasing compression rates. The value of the top of each image corresponds to the SSIM measure with respect to the ground truth and the value on the bottom correspond to the compression rate. We can observe that increasing the compression-rate-based decomposition eliminates noise significantly and results in the reconstructed image to resemble the original noise-free image. For regular TT/SVD-TT based reconstruction, the best SSIM reported for the reconstructed image is 0.85 whereas with the non-negative TT/nTT based reconstruction, the best SSIM reported is 0.88. For given TT ranks, the reconstructed image SSIM for nTT is better than that for the TT.

4) Compression of large synthetic data: We demonstrate the compression ratios with lower reconstruction error for a 500 Gigabyte (GB) matrix with dimensions $1024 \times 512 \times 512 \times 512$ and tensor train ranks =[1,20,30,40,1]. We synthetically generate the data in a distributed manner as discussed in the data generation section. Figure 8c shows compression ratios with two different NMF optimization methods, BCD vs multiplicative update, both of which are based on minimization of the Frobenius norm. For the BCD optimization-based NTF, the compression ratio C varies from 163880 with $\epsilon = 3e-6$ to C of 6391320 for $\epsilon = 0.03$ with non-negative tensor train. Similarly, with multiplicative update algorithm based NTF, the relative error ϵ varies from 0.005 to 0.045 for the same compression range. This experiment demonstrates the tradeoff between two different NMF update algorithms BCD and MU for nTT. As per the scaling plots 5,6 and 7, MU algorithm demonstrates better timings. However, BCD achieves a better

compression rate with lower reconstruction error compared to MU as per Figure 8c.

V. Conclusion and Future directions

Here, we introduce a distributed non-negative tensor train, nTT, algorithm that is capable of computing tensor train to a prescribed relative error. We demonstrate the nTT scaling performance on synthetic data, and establish its ability to decompose a 500GB tensor. Finally, we apply the algorithm to various real and synthetic datasets to demonstrate the nTT data compression capabilities. In the future, we aim to apply our framework to large real-world datasets such as seismic datasets, satellite images, medical images, etc., in order to have an efficient highly compressed representation and to be able to do inference/classification from the nTT low-dimensional representations.

VI. Acknowledgements

This research was funded by Laboratory Directed Research and Development (20190020DR), and resources were provided by the Los Alamos National Laboratory Institutional Computing Program, supported by the U.S. Department of Energy National Nuclear Security Administration under Contract No. 89233218CNA000001.

References

[1] L. R. Tucker, "Some mathematical notes on three-mode factor analysis," *Psychometrika*, vol. 31, no. 3, pp. 279–311, 1966. 1

[2] F. L. Hitchcock, "The expression of a tensor or a polyadic as a sum of products," *Journal of Mathematics and Physics*, vol. 6, no. 1-4, pp. 164–189, 1927. 1

[3] J. Håstad, "Tensor rank is np-complete," *Journal of algorithms (Print)*, vol. 11, no. 4, pp. 644–654, 1990. 1

[4] V. De Silva and L.-H. Lim, "Tensor rank and the ill-posedness of the best low-rank approximation problem," *SIAM Journal on Matrix Analysis and Applications*, vol. 30, no. 3, pp. 1084–1127, 2008. 1

[5] W. Austin, G. Ballard, and T. G. Kolda, "Parallel tensor compression for large-scale scientific data," in *International parallel and distributed processing symposium*. IEEE, 2016, pp. 912–922. 1

[6] I. Oseledets, "A new tensor decomposition," in *Doklady Mathematics*, vol. 80, no. 1. Pleiades Publishing, Ltd, 2009, pp. 495–496. 1, 2, 3

[7] I. V. Oseledets, "Tensor-train decomposition," *SIAM Journal on Scientific Computing*, vol. 33, no. 5, pp. 2295–2317, 2011. 1, 2

[8] Z. Li and P. Zhang, "Shortcut matrix product states and its applications," *arXiv preprint arXiv:1812.05248*, 2018. 1

[9] W. Wang, V. Aggarwal, and S. Aeron, "Principal component analysis with tensor train subspace," *Pattern Recognition Letters*, vol. 122, pp. 86–91, 2019. 1, 7

[10] M. Ishteva, "Tensors and latent variable models," in *International Conference on Latent Variable Analysis and Signal Separation*. Springer, 2015, pp. 49–55. 2

[11] E. Robeva and A. Seigal, "Duality of graphical models and tensor networks," *Information and Inference: A Journal of the IMA*, vol. 8, no. 2, pp. 273–288, 2019. 2

[12] L.-H. Lim and P. Comon, "Nonnegative approximations of nonnegative tensors," *Journal of Chemometrics: A Journal of the Chemometrics Society*, vol. 23, no. 7-8, pp. 432–441, 2009. 2

[13] Y. Qi, P. Comon, and L.-H. Lim, "Semialgebraic geometry of nonnegative tensor rank," *SIAM Journal on Matrix Analysis and Applications*, vol. 37, no. 4, pp. 1556–1580, 2016. 2

[14] C. Eckart and G. Young, "The approximation of one matrix by another of lower rank," *Psychometrika*, vol. 1, no. 3, pp. 211–218, 1936. 2

[15] A. Novikov, P. Izmailov, V. Khrulkov, M. Figurnov, and I. Oseledets, "Tensor train decomposition on tensorflow (t3f)," *Journal of Machine Learning Research*, vol. 21, no. 30, pp. 1–7, 2020. 2

[16] J. Kossaifi, Y. Panagakis, A. Anandkumar, and M. Pantic, "Tensorly: Tensor learning in python," *The Journal of Machine Learning Research*, vol. 20, no. 1, pp. 925–930, 2019. 2

[17] M. Ding, T.-Z. Huang, X.-L. Zhao, M. K. Ng, and T.-H. Ma, "Tensor train rank minimization with nonlocal self-similarity for tensor completion," *arXiv preprint arXiv:2004.14273*, 2020. 2

[18] S. Holtz, T. Rohwedder, and R. Schneider, "The alternating linear scheme for tensor optimization in the tensor train format," *SIAM Journal on Scientific Computing*, vol. 34, no. 2, pp. A683–A713, 2012. 2

[19] T. Huckle, K. Waldherr, and T. Schulte-Herbrüggen, "Computations in quantum tensor networks," *Linear Algebra and its Applications*, vol. 438, no. 2, pp. 750–781, 2013. 2

[20] K. H. Marti, B. Bauer, M. Reiher, M. Troyer, and F. Verstraete, "Complete-graph tensor network states: a new fermionic wave function ansatz for molecules," *New Journal of Physics*, vol. 12, no. 10, p. 103008, 2010. 2

[21] K. Fonał and R. Zdunek, "Distributed and randomized tensor train decomposition for feature extraction," in *2019 International Joint Conference on Neural Networks (IJCNN)*. IEEE, 2019, pp. 1–8. 2

[22] X. Wang, L. T. Yang, Y. Wang, X. Liu, Q. Zhang, and M. J. Deen, "A distributed tensor-train decomposition method for cyber-physical-social services," *ACM Transactions on Cyber-Physical Systems*, vol. 3, no. 4, pp. 1–15, 2019. 2

[23] X. Wang, L. T. Yang, Y. Wang, L. Ren, and M. J. Deen, "Adtt: A highly-efficient distributed tensor-train decomposition method for iiot big data," *IEEE Transactions on Industrial Informatics*, 2020. 2

[24] H. Carrillo-Cabada, E. Skau, G. Chennupati, B. Alexandrov, and H. Djidjev, "An out of memory tsvd for big-data factorization," *IEEE Access*, vol. 8, pp. 107 749–107 759, 2020. 2

[25] N. Lee, A.-H. Phan, F. Cong, and A. Cichocki, "Nonnegative tensor train decompositions for multi-domain feature extraction and clustering," in *International Conference on Neural Information Processing*. Springer, 2016, pp. 87–95. 3

[26] E. Shcherbakova, "Nonnegative tensor train factorization with dmrg technique," *Lobachevskii Journal of Mathematics*, vol. 40, no. 11, pp. 1863–1872, 2019. 3

[27] E. Shcherbakova and E. Tyrtyshnikov, "Nonnegative tensor train factorizations and some applications," in *International Conference on Large-Scale Scientific Computing*. Springer, 2019, pp. 156–164. 3

[28] I. V. Oseledets and E. E. Tyrtyshnikov, "Breaking the curse of dimensionality, or how to use svd in many dimensions," *SIAM Journal on Scientific Computing*, vol. 31, no. 5, pp. 3744–3759, 2009. 3

[29] T. G. Kolda and B. W. Bader, "Tensor decompositions and applications," *SIAM review*, vol. 51, no. 3, pp. 455–500, 2009. 3

[30] O. Roy and M. Vetterli, "The effective rank: A measure of effective dimensionality," in *2007 15th European Signal Processing Conference*. IEEE, 2007, pp. 606–610. 4

[31] C. M. Bishop, "Bayesian pca," in *Advances in neural information processing systems*, 1999, pp. 382–388. 4

[32] G. Chennupati, R. Vangara, E. Skau, H. Djidjev, and B. Alexandrov, "Distributed non-negative matrix factorization with determination of the number of latent features," *The Journal of Supercomputing*, pp. 1–31, 2020. 4, 5

[33] Y. Xu and W. Yin, "A block coordinate descent method for regularized multiconvex optimization with applications to nonnegative tensor factorization and completion," *SIAM Journal on imaging sciences*, vol. 6, no. 3, pp. 1758–1789, 2013. 5

[34] A. Georghiades, P. Belhumeur, and D. Kriegman, "From few to many: Illumination cone models for face recognition under variable lighting and pose," *IEEE Trans. Pattern Anal. Mach. Intelligence*, vol. 23, no. 6, pp. 643–660, 2001. 7

[35] W. Wang, V. Aggarwal, and S. Aeron, "Efficient low rank tensor ring completion," in *Proceedings of the IEEE International Conference on Computer Vision*, 2017, pp. 5697–5705. 7

[36] Discovery, "Pistol shot recorded at 73,000 frames per second," https://youtu.be/7y9apnbI6GA, Aug 2015. 7

[37] W. Clifton, A. Frank, and S.-m. Freeman, "Osteopetrosis (marble bones)," *Am. J. Dis. Child*, vol. 56, no. 2, pp. 1020–1936, 1938. 8